Particle Trajectories, Heating, and Breakup in Hypersonic Shock Layers

G. D. WALDMAN* AND W. G. REINECKE†
Avco Systems Division, Wilmington, Mass.

An analysis is made of the motion of small, spherical, noninteracting solid or liquid particles through hypersonic flowfields over spheres and cones. It is shown that the motion of the particles depends only on the density ratio across the shock and a dimensionless ballistic parameter. Approximate solutions to the particle equations of motion are obtained in closed form in terms of these parameters for two flow configurations, a sharp cone and the stagnation region of a sphere. A technique is derived for the determination of the aerodynamic heating and melting (or vaporization) of the particles as they traverse the shock layer. Results for the particle mass loss as a result of heating are presented for the stagnation region, the more severe heating environment. Existing correlations of experimental data on the breakup of drops due to aerodynamic forces are used to predict the extent of raindrop breakup in the shock layer.

Nomenclature

A = cross-sectional area of particle
C_D = drag coefficient of particle based on area A, assumed constant
f,g,F,G = flow and particle velocity perturbations defined by Eq. (5)
h = gas density perturbation defined by Eq. (5)
H_e = dimensionless heating rate group defined by Eq. (43)
K_s = ballistic coefficient for stagnation region defined by Eq. (4)
K_c = ballistic coefficient for conical region defined by Eq. (23)
L = thickness of conical shock layer
m = mass of particle
q = average heat-transfer rate over front surface of particle
q_{stag} = stagnation-point heat-transfer rate of particle
Q = heat capacity plus latent heat of fusion of particle
r = particle radius, μ
R,θ = polar coordinates (see Fig. 1)
$\bar{R}$ = R/R_i (conical region)
R_N = nose radius
t = time from entry of particle into shock layer
u,v = flow velocity components in R, θ directions
U,V = particle velocity components in R, θ directions: $u = dR/dt$, $V = Rd\theta/dt$
$\bar{u},\bar{v},\bar{U},\bar{V}$ = flow and particle velocity components nondimensionalized by V_∞
V_∞ = freestream velocity
w = relative velocity $[(U-u)^2 + (V-v)^2]^{1/2}$
$\bar{w}$ = w/V_∞
y = nondimensionalized independent variable defined by Eq. (2)
β = impact angle (see Fig. 1)
Δ = bow shock wave standoff distance on stagnation line
ϵ = shock wave density ratio (ρ_∞/ρ_{s0} for stagnation region, ρ_∞/ρ_s for conical region)
ρ = gas density
ρ_0 = 2.498×10^{-3} slugs/ft^3
ρ_s = gas density behind bow shock wave
ρ_{s0} = gas density behind bow shock wave evaluated at axis of symmetry
$\bar{\rho}$ = ρ/ρ_{s0} for stagnation region; ρ/ρ_s for conical region
σ = density of particle material
θ_c = cone half-angle
$\bar{\theta}$ = angular independent variable defined by Eq. (21)

Subscripts

e = conditions at entry of particle into shock layer
i = at body surface; at impact
s = behind bow shock wave at point where particle enters shock layer
SL = along stagnation line
0,1,2 = coefficients in expansion in powers of $\epsilon^{1/2}$ (stagnation region) or ϵ (conical region)
∞ = freestream conditions

Shock tube notation used in Sec. IV

b = ρ_∞/σ
s = distance between particle and shock wave
u_S = shock wave velocity
u_2,ρ_2 = flow velocity and density behind shock wave
x = distance which particle has moved

Presented as Paper 69-712 at the AIAA Fluid and Plasma Dynamics Conference, San Francisco, Calif., June 16–18, 1969; submitted October 23, 1969; revision received December 22, 1970.

* Senior Consulting Scientist, Flight Mechanics Department. Member AIAA.
† Fluid Physics Department. Member AIAA.

I. Introduction

A VEHICLE flying through the atmosphere may encounter suspended particles of water, ice or dust, and it is of interest to determine in what way the flowfield around the body influences these particles. In general, the particles will be decelerated, deflected, melted, and, if they are initially liquid, shattered by the gas flow about the moving body. The deceleration and deflection effects have been studied in incompressible flow by Taylor.[1] The present authors examined these effects for compressible flow (most recently in Ref. 2) using an approach somewhat similar to that adopted in Sec. II below. Probstein and Fassio[3] subsequently studied the same problem, but invoked the assumption of constant-density flow.

In the present paper, the effects of deceleration, deflection, melting, and shattering will be analyzed for spherical and conical bodies in compressible flow. The analysis of the flowfield effects for the sphere is limited to the stagnation region. Approximate, closed-form solutions are obtained in each case for the trajectories of the overtaken particles. These solutions are then used to analyze the melting of particles along the stagnation line of the sphere. Finally, relevant experimental data[4,5] are employed to calculate the shattering of initially liquid particles for both the sphere and cone.

The emphasis here has been to obtain general, closed-form solutions that are amenable to slide rule calculations. To illustrate the results, numerical calculations are made of

shock-layer effects for a body flying through sand and ice particles and rain.

Throughout the paper, it is assumed that the suspended particles are spherical with uniform density, noninteracting, and present in sufficiently low concentration so as not to alter the flowfield around the moving body.

It is further assumed that the drag coefficient C_D of the particles is a constant independent of particle size, velocity, and flow density. This is a reasonable assumption in view of the relatively large Reynolds numbers and Mach numbers of particles with radii greater than 5 μ, which is the size range of physical interest. In the numerical calculations cited, the Reynolds number for particles behind the normal shock in the stagnation region is 580 r, where r is the particle radius in microns, and the Mach number is 2.5. Behind the conical shock, the Reynolds number is 110 r and the relative Mach number is 1.

II. Particle Trajectories

Stagnation Region

In the stagnation region, we express the equations of motion in polar coordinates (R, θ) with the origin at the center of curvature of the bow shock on the line of symmetry (Fig. 1). The corresponding flow velocity components are denoted (u,v), and the particle velocity components are denoted (U,V). The equations of motion for a particle expressed in this coordinate system are

$$m[dU/dt - V^2/R] = -\tfrac{1}{2}C_D A\rho w(U - u) \quad (1a)$$

$$m[dV/dt + UV/R] = -\tfrac{1}{2}C_D A\rho w(V - v) \quad (1b)$$

where $w = [(U-u)^2 + (V-v)^2]^{1/2}$ is the relative velocity between the particle and the flow. We introduce dimensionless velocity components $\bar{u}$, etc. and density $\bar{\rho}$, nondimensionalized by V_∞, the magnitude of freestream velocity, and ρ_{s0}, the density behind the shock on the line of symmetry (stagnation line). We will employ a nondimensionalized independent variable

$$y = (R_S - R)/\Delta \quad (2)$$

We will assume, consistent with the hypersonic flowfield approximation made below, that the shock and body are concentric, so that $R_S = R_N + \Delta$. Expressing Eq. (1) in terms of these variables and replacing t by y as the independent variable, we obtain

$$\bar{U}\frac{d\bar{U}}{dy} + \frac{\Delta}{R_N}\frac{\bar{V}^2}{1 + (\Delta/R_N)(1-y)} = K_S\bar{\rho}\bar{w}(\bar{U} - \bar{u}) \quad (3a)$$

$$\bar{U}\frac{d\bar{V}}{dy} - \frac{\Delta}{R_N}\frac{\bar{U}\bar{V}}{1 + (\Delta/R_N)(1-y)} = K_S\bar{\rho}\bar{w}(\bar{V} - \bar{v}) \quad (3b)$$

where

$$K_S = C_D A\rho_{S0}\Delta/2m$$

For a spherical particle with uniform density σ and radius r,

$$K_S = 3C_D\rho_{S0}\Delta/8\sigma r \quad (4)$$

In the vicinity of the stagnation line, Eqs. (3) can be solved by expressing the variables in appropriate power series in the angular variable θ:

$$\bar{u} = \bar{u}_{SL}(y) + \theta^2 f(y) + \ldots, \quad \bar{v} = \theta g(y) + \ldots$$

$$\bar{\rho} = \bar{\rho}_{SL}(y) + \theta^2 h(y) + \ldots$$

$$\bar{U} = \bar{U}_{SL}(y) + \theta^2 F(y) + \ldots, \quad \bar{V} = \theta G(y) + \ldots \quad (5)$$

Substituting and separating out powers of θ, we obtain for the leading terms

$$\bar{U}_{SL}(d\bar{U}_{SL}/dy) = -K_S\bar{\rho}_{SL}(\bar{U}_{SL} - \bar{u}_{SL})^2 \quad (6a)$$

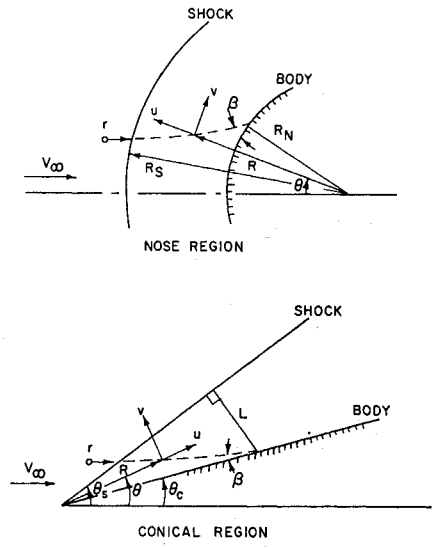

Fig. 1 Coordinate system.

$$\bar{U}_{SL}\frac{dF}{dy} + F\frac{d\bar{U}_{SL}}{dy} + \frac{\Delta}{R_N}\frac{G(G-2F)}{1 + (\Delta/R_N)(1-y)} = -K_S\{\bar{\rho}_{SL}[2(\bar{U}_{SL} - \bar{u}_{SL})(F - f) + \tfrac{1}{2}(G-g)^2] + h(\bar{U}_{SL} - \bar{u}_{SL})^2\} \quad (6b)$$

$$\bar{U}_{SL}\frac{dG}{dy} - \frac{\Delta}{R_N}\frac{G(G + \bar{U}_{SL})}{1 + (\Delta/R_N)(1-y)} = -K_S\bar{\rho}_{SL}(\bar{U}_{SL} - \bar{u}_{SL})(G - g) \quad (6c)$$

Equations (6) can be solved in closed form if we make certain reasonable assumptions on the behavior of the flowfield variables and the solution itself. Let ϵ be the shock density ratio on the stagnation line. The shock near the stagnation line will be taken to be a sphere. We shall approximate $\bar{u}$, $\bar{v}$, and $\bar{\rho}$ by linear functions of y satisfying the boundary conditions at the shock ($y = 0$) and at the surface of the body ($y = 1$):

$$\bar{u}_{SL} = -\epsilon(1-y), \quad \bar{\rho}_{SL} = 1 + \epsilon\xi_\rho y$$

$$f = \epsilon(\tfrac{1}{2} - \xi_1)(1-y), \quad g = 1 - y + \epsilon^{1/2}\xi_v y$$

$$h = -[\xi_1 + (\xi_2 - \xi_1)y] \quad (7)$$

where

$$\xi_\rho = [(\bar{\rho}_{SL})_i - 1]/\epsilon = [(\rho_{SL})_i - (\rho_{SL})_S]/\rho_\infty$$

$$\xi_1 = -\tfrac{1}{2}[(\partial^2/\partial\theta^2)(\bar{\rho}_s)]_{SL}, \quad \xi_2 = -\tfrac{1}{2}[(\partial^2/\partial\theta^2)(\bar{\rho}_i)]_{SL}$$

$$\xi_v = -(1/\epsilon^{1/2})[(\partial/\partial\theta)(\bar{v}_i)]_{SL}$$

The standoff distance, assumed independent of θ, is given by the equation

$$\Delta/R_N = \epsilon\xi_\Delta \quad (8)$$

Equations (7) imply an ordering of the various quantities with respect to the density ratio ϵ. The quantities ξ_ρ, ξ_1, ξ_2, and ξ_v can, in principle, be determined from a limiting theory such as constant-density theory or the constant-streamtube-area flow model, but it will generally be preferable to evaluate them from numerical flow solutions or experimental data. Hence Eqs. (7) are not necessarily associated with any theoretical flow model. Based on numerical solutions, a representative value of ξ_ρ is $\frac{1}{2}$. For a perfect gas, $\xi_1 = 2/[(\gamma-1)M_\infty^2 + 2]$ and is therefore small at high Mach numbers. The value of ξ_v is given quite accurately by 2. For a perfect gas,

$$\xi_2 \simeq \xi_v^2/(\gamma+1) \simeq 2/(\gamma+1)$$

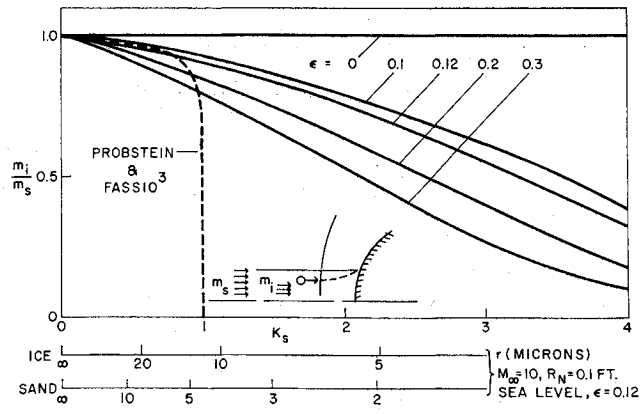

Fig. 2 Capture area ratio for spherical nose.

From flowfield solutions for spheres,[6,7] $\Delta/\epsilon R_N \simeq 0.78$, and we shall use this value for ξ_Δ.

We shall now make the high-speed approximation that ϵ is small, so that the solution for the particle trajectory can be expanded in a series in $\epsilon^{1/2}$:

$$\bar{U}_{SL} = \bar{U}_0 + \epsilon U_2 + \ldots, \quad F = F_0 + \epsilon^{1/2}F_1 + \epsilon F_2 + \ldots$$
$$G = G_0 + \epsilon^{1/2}G_1 + \epsilon G_2 + \ldots \tag{9}$$

We substitute Eqs. (7–9) into Eqs. (6), expand, and equate powers of ϵ^0, $\epsilon^{1/2}$, etc. From the ϵ^0 terms, we have

$$\bar{U}_0(d\bar{U}_0/dy) = -K_S\bar{U}_0^2 \tag{10a}$$

$$\bar{U}_0\frac{dF_0}{dy} + F_0\frac{d\bar{U}_0}{dy} = -K_S\{2\bar{U}_0F_0 + \tfrac{1}{2}(G_0 - 1 + y)^2 - \bar{U}_0^2[\xi_1 + (\xi_2 - \xi_1)y]\} \tag{10b}$$

$$\bar{U}_0(dG_0/dy) = -K_S\bar{U}_0(G_0 - 1 + y) \tag{10c}$$

The $\epsilon^{1/2}$ terms yield

$$\bar{U}_0\frac{dF_1}{dy} + F_1\frac{d\bar{U}_0}{dy} = -K_s[2\bar{U}_0F_1 + (G_0 - 1 + y)(G_1 - \xi_v y)] \tag{11a}$$

$$\bar{U}_0 dG_1/dy = -K_s\bar{U}_0(G_1 - \xi_v y) \tag{11b}$$

These equations are subject to the following boundary conditions at the shock ($y = 0$):

$$\bar{U}_0(0) = -1, \quad F_0(0) = \tfrac{1}{2}, \quad G_0(0) = 1$$
$$F_1(0) = 0, \quad G_1(0) = 0 \tag{12}$$

Subject to these conditions, the solutions to Eqs. (10) and (11) are as follows. For the ϵ° terms,

$$\bar{U}_0 = -e^{-K_s y} \tag{13a}$$

$$F_0 = (1/4K_s^2)\{e^{K_s y} - 4 + [2K_s^2 + 3 + 2K_s(1 - 2K_s^2\xi_1)y + 2K_s^3(\xi_1 - \xi_2)y^2]e^{-K_s y}\} \tag{13b}$$

$$G_0 = (1/K_s)(1 - e^{-K_s y}) + 1 - y \tag{13c}$$

For the $\epsilon^{1/2}$ terms,

$$F_1 = -(\xi_v/2K_s^2)[e^{K_s y} - 4 + (2K_s y + 3)e^{-K_s y}] \tag{14a}$$

$$G_1 = (\xi_v/K_s)(K_s y - 1 + e^{-K_s y}) \tag{14b}$$

The trajectory of a particle can be obtained from the equation

$$R(d\theta/dR) = V/U \tag{15}$$

Substituting, we have

$$\frac{d\theta}{\theta dy} = -\frac{\Delta}{R_N + \Delta(1 - y)}\frac{G}{\bar{U}_{SL}} + 0(\theta^2) = -\epsilon\xi_\Delta\left(\frac{G_0}{\bar{U}_0} + \epsilon^{1/2}\frac{G_1}{\bar{U}_0}\right) + 0(\theta^2,\epsilon^2) \tag{16}$$

We shall make the substitution $\bar{\theta} = \theta/\theta_s$, where θ_s is the value of θ at the point of entry into the shock layer, and expand in ϵ and θ_s^2:

$$\bar{\theta} = 1 + \epsilon[\bar{\theta}_0 + \epsilon^{1/2}\bar{\theta}_1 + \ldots + 0(\bar{\theta}_s^2) + \ldots] \tag{17}$$

By substituting in Eq. (16), equating terms of the same order in ϵ, and integrating, we have derived the first two terms in the expansion:

$$\bar{\theta}_0 = -(\xi_\Delta/K_s^2)\{K_s(1 + y) + 2 - [K_s(1 - y) + 2]e^{K_s y}\} \tag{18a}$$

$$\bar{\theta}_1 = (\xi_\Delta\xi_v/K_s^2)[K_s y + 2 + (K_s y - 2)e^{K_s y}] \tag{18b}$$

The values of the various quantities at impact are found by taking $y = 1$ in the preceding equations. Of particular interest are the impact angle and the ratio of the impinging particle mass to the mass that would strike the surface in the absence of a shock layer, dubbed the "capture area ratio" in the authors' previous work and the "collection efficiency" in Ref. 3. The capture area ratio is given by

$$\frac{m_i}{m_s} = \left(\frac{R_s\sin\theta_s}{R_N\sin\theta_i}\right)^2 = \left[\frac{1 + \epsilon\xi_\Delta}{1 + \epsilon(\bar{\theta}_0)_i + \epsilon^{3/2}(\bar{\theta}_1)_i}\right]^2 + 0(\epsilon^2,\theta_s^2) = \left[\frac{1 + \epsilon\xi_\Delta}{1 + (\epsilon\xi_\Delta/K_s^2)\{2(e^{K_s} - K_s - 1) + \xi_v\epsilon^{1/2}[(K_s - 2)e^{K_s} + K_s + 2]\}}\right]^2 + \ldots \tag{19}$$

This quantity is plotted in Fig. 2 to the indicated order of approximation along with the result of Ref. 3 (in Ref. 3, β_i corresponds to the reciprocal of our K_s).

In contrast to the theory of Probstein and Fassio,[3] the capture area ratio does not show an abrupt cutoff as a function of K_s, and does not vanish for any particles. In addition, there is a substantial variation with ϵ as well as K_s. These discrepancies may be accounted for by the approximation $|\bar{U}| \gg |\bar{u}|$ (in our notation) made in Ref. 3, which invalidates the results in that paper for particles small enough to be appreciably decelerated. Clearly, all particles, no matter how small, which are not melted or shattered, must strike the body in this region.

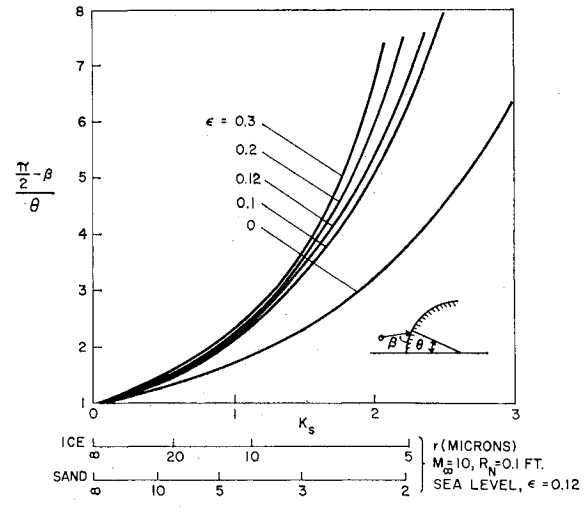

Fig. 3 Impact angle variation for spherical nose.

The impact angle is defined by the equation

$$\beta = \tan^{-1}\left(-\frac{U}{V}\right)_i = \frac{\pi}{2} + \theta\left(\frac{G}{\bar{U}_{SL}}\right)_i + 0(\theta^3) = \frac{\pi}{2} + \theta\left(\frac{G_0 + \epsilon^{1/2}G_1}{\bar{U}_0}\right)_i + 0(\epsilon\theta,\theta^3) =$$

$$\frac{\pi}{2} - \frac{\theta}{K_s}\{e^{K_s} - 1 + \epsilon^{1/2}\xi_u[(K_s - 1)e^{K_s} + 1]\} + \ldots \quad (20)$$

In Fig. 3 we have plotted $(\pi/2 - \beta)/\theta$, which is unity for an undeflected particle.

Conical Region

Sufficiently far downstream of the stagnation region, the shock layer becomes approximately conical. The polar coordinate system (R,θ) for a conical shock layer is illustrated in Fig. 1. The principal effect of the conical shock layer in the present context is to deflect the particles away from the surface, since the axial deceleration of the particles is small and there is insufficient relative velocity to cause appreciable heating and melting, at least for sand particles.[2] We shall therefore be concerned with the reduction in the impact angle β measured from the vehicle surface (Fig. 1), which in the absence of a shock layer is equal to the cone half-angle θ_c.

The equations of motion for a particle expressed in this coordinate system are identical to Eqs. (1). We introduce dimensionless velocity components as before, defining $\bar{\rho} = \rho/\rho_s$, $\bar{R} = R/R_i$, and define a new angular variable

$$\bar{\theta} = (\theta_s - \theta)/(\theta_s - \theta_c) \quad (21)$$

Here R_i is the radial coordinate of the impact point. We express Eqs. (1) in terms of these variables and replace t by $\bar{\theta}$ as the independent variable:

$$(\bar{V}/\bar{R})[d\bar{U}/d\bar{\theta} + (\theta_s - \theta_c)\bar{V}] = K_c\bar{\rho}\bar{w}(\bar{U} - \bar{u}) \quad (22a)$$

$$(\bar{V}/\bar{R})[d\bar{V}/d\bar{\theta} - (\theta_s - \theta_c)\bar{U}] = K_c\bar{\rho}\bar{w}(\bar{V} - \bar{v}) \quad (22b)$$

where

$$K_c = C_D A\rho_s R_i(\theta_s - \theta_c)/2m = 3C_D\rho_s R_i(\theta_s - \theta_c)/8\sigma r \quad (23)$$

As in the stagnation region, we shall approximate the flow-field variables $\bar{u}$, $\bar{v}$, $\bar{\rho}$ by linear functions in $\bar{\theta}$ satisfying the boundary conditions at the shock ($\bar{\theta} = 0$) and at the vehicle surface ($\bar{\theta} = 1$):

$$\bar{u} = \bar{u}_s - \epsilon\lambda_u\bar{\theta}, \quad \bar{v} = -\epsilon\sin\theta_c(1 - \bar{\theta})$$

$$\bar{\rho} = 1 + \epsilon\lambda_\rho\bar{\theta} \quad (24)$$

where

$$\lambda_u = (\bar{u}_s - \bar{u}_i)/\epsilon = (\cos\theta_s - \bar{u}_i)/\epsilon$$

$$\lambda_\rho = (\bar{\rho}_i - 1)/\epsilon = (\rho_i - \rho_s)/\rho_\infty$$

By examining appropriate conical flow solutions, it can be verified that these are very adequate approximations to the actual behavior of the flow variables.[2] Furthermore, since the shock layer thickness $(\theta_s - \theta_c)$ is proportional to the density ratio $\epsilon = \rho_\infty/\rho_s$, we define λ_θ by the equation

$$(\theta_s - \theta_c)/\theta_s = \epsilon\lambda_\theta \quad (25)$$

Representative values are $\lambda_u \cong 0$ and $\lambda_\rho \cong 0.212$. The quantity λ_θ varies somewhat over the range of interest, but an average value of 0.6 can be employed for $\epsilon < \frac{1}{2}$. (In constant-density theory, $\lambda_\theta \to 0.5$ for small cone angles.)

We make the high-speed approximation that ϵ is small, and expand the drop velocity components in powers of ϵ:

$$\bar{U} = \bar{U}_0 + \epsilon\bar{U}_1 + \epsilon^2\bar{U}_2 + \ldots \quad (26a)$$

$$\bar{V} = \bar{V}_0 + \epsilon\bar{V}_1 + \epsilon^2\bar{V}_2 + \ldots \quad (26b)$$

Since in the limit $\epsilon \to 0$, $\bar{R} \to 1$, an expansion for the radial coordinate analogous to Eqs. (26) is

$$\bar{R} = 1 + \epsilon\bar{R}_1 + \epsilon^2\bar{R}_2 + \ldots \quad (27)$$

where each coefficient of ϵ is understood to be a function of θ. We will verify later that Eq. (27) is the appropriate expansion.

Substituting Eqs. (24–27) into Eqs. (22), expanding, and equating powers of ϵ, we find that the first two components satisfy the equations

$$\bar{V}_0(d\bar{U}_0/d\bar{\theta}) = K_c\bar{w}_0(\bar{U}_0 - \cos\bar{\theta}_c) \quad (28)$$

$$\bar{V}_0(d\bar{V}_0/d\bar{\theta}) = K_c\bar{w}_0\bar{V}_0 \quad (29)$$

$$V_0(d\bar{U}_1/d\bar{\theta}) + (d\bar{U}_0/d\bar{\theta}_1)\bar{V}_1 - K_c[\bar{w}_0\bar{U}_1 + (\bar{U}_0 - \cos\theta_c)\bar{w}_1] = K_c\bar{w}_0[\lambda_u\bar{\theta} + \lambda_\theta\theta_c\sin\theta_c + (\bar{U}_0 - \cos\theta_c)(\bar{R}_1 + \lambda_\rho\bar{\theta})] - \lambda_\theta\theta_c\bar{V}_0^2 \quad (30)$$

$$\bar{V}_0(d\bar{V}_1/d\bar{\theta}) + (d\bar{V}_0/d\bar{\theta} - K_c\bar{w}_0)\bar{V}_1 - K_c\bar{V}_0\bar{w}_1 = K_c\bar{w}_0[\sin\theta_c(1 - \bar{\theta}) + \bar{V}_0(\bar{R}_1 + \lambda_\rho\bar{\theta}) + \lambda_\theta\theta_c\bar{U}_0\bar{V}_0 \quad (31)$$

where

$$\bar{w}_0 = [(\bar{U}_0 - \cos\theta_c)^2 + \bar{V}_0^2]^{1/2}$$

$$\bar{w}_1 = (1/\bar{w}_0)\{(\bar{U}_0 - \cos\theta_c)(\bar{U}_1 + \lambda_u\bar{\theta} + \lambda_\theta\theta_c\sin\theta_c) + \bar{V}_0[\bar{V}_1 + \sin\theta_c(1 - \bar{\theta})]\}$$

Here, in contrast to the stagnation region, we have retained terms of order ϵ^1 since ϵ is larger for given freestream conditions.

The solution of Eq. (28), consistent with the boundary condition at the shock, is

$$\bar{U}_0 = \cos\theta_c \quad (32)$$

Equation (29) then has the solution

$$\bar{V}_0 = -e^{-K_c\bar{\theta}}\sin\theta_c \quad (33)$$

By expanding Eq. (15) in powers of ϵ and invoking the boundary conditions on $\bar{R}$ at the surface, we see that the expansion (27) for $\bar{R}$ is correct. The functions $\bar{R}_1$ and $\bar{R}_2$ are determined from the first- and second-order components of Eq. (15):

$$d\bar{R}_1/d\bar{\theta} = -\lambda_\theta\theta_c\bar{U}_0/\bar{V}_0$$

$$d\bar{R}_2/d\bar{\theta} = \bar{R}_1 d\bar{R}_1/d\bar{\theta} - (\lambda_\theta\theta_c/\bar{V}_0)[\bar{U}_1 - \bar{U}_0\bar{V}_1/\bar{V}_0 + \lambda_\theta\bar{U}_0]$$

yielding

$$\bar{R}_1 = -(\lambda_\theta\theta_c\cot\theta_c/K_c)(e^{K_c} - e^{K_c\bar{\theta}}) \quad (34a)$$

$$\bar{R}_2 = (\lambda_\theta\theta_c\cot\theta_c/K_c^2)[(1 - \lambda_\theta\theta_c\cot\theta_c)\{[\tfrac{3}{2}(e^{K_c} + e^{K_c\bar{\theta}}) - 2(K_c + 1)](e^{K_c} - e^{K_c\bar{\theta}}) - K_c(1 - \bar{\theta})e^{2K_c\bar{\theta}}\} + K_c\lambda_\theta\{[\theta_c\tan\theta_c - 1 + (e^{K_c} + \{1 - \bar{\theta}\}e^{K_c\bar{\theta}} - 1)\theta_c \times \cot\theta_c](e^{K_c} - e^{K_c\bar{\theta}}) - (K_c/2)(1 - \bar{\theta}^2)\theta_c\tan\theta_c\} + (\lambda_u/\cos\theta_c)\{(K_c - 2)(e^{K_c} - e^{K_c\bar{\theta}}) + K_c(1 - \bar{\theta})(1 + e^{K_c\bar{\theta}})\} - (\lambda_\rho/2)\{(K_c^2 - 2K_c + 2)(e^{K_c} - e^{K_c\bar{\theta}}) + K_c(1 - \bar{\theta})[K_c(1 + \bar{\theta}) - 2]e^{K_c\bar{\theta}}\}] \quad (34b)$$

Substituting into Eqs. (30) and (31), integrating, and applying the appropriate boundary conditions at the shock, we obtain

$$\bar{U}_1 = -(\lambda_u/K_c)(K_c\bar{\theta} - 1 + e^{-K_c\bar{\theta}}) + \lambda_\theta\theta_c\sin\theta_c(\bar{\theta}e^{-K_c\bar{\theta}} - 1) \quad (35a)$$

$$\bar{V}_1 = -(2\sin\theta_c/K_c)[(K_c + 1)(1 - e^{-K_c\bar{\theta}}) - K_c\bar{\theta}] + (\lambda_\rho\sin\theta_c/2)K_c\bar{\theta}^2e^{-K_c\bar{\theta}} + (\lambda_\theta\theta_c\cos\theta_c/K_c) \times [2 - (K_c + 2 + K_c\bar{\theta}e^{K_c})e^{-K_c\bar{\theta}}] \quad (35b)$$

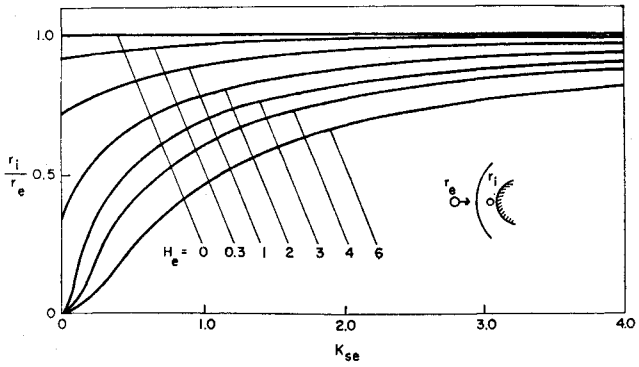

Fig. 4 Particle radius at impact, including mass loss by heating.

To obtain conditions at impact, we evaluate Eqs. (32–35) at $\bar{\theta} = 1$. The capture area ratio is

$$m_i/m_s = (R_s \sin\theta_s/R_i \sin\theta_c)^2 \cong$$
$$[1 + \epsilon\lambda_\theta\theta_c \cot\theta_c + \epsilon^2\lambda_\theta^2\theta_c (\cot\theta_c - \theta_c/2^2] \times$$
$$[1 + \epsilon\bar{R}_1(0) + \epsilon^2\bar{R}_2(0)]^2 \quad (36)$$

The quantity of primary interest, the impact angle, can be determined from the equation

$$\beta = \tan^{-1}\left(-\frac{\bar{V}}{\bar{U}}\right)_i =$$
$$\left[\tan^{-1}\left(-\frac{\bar{V}_0}{\bar{U}_0}\right)_i - \epsilon\frac{\bar{V}_0}{\bar{U}_0}\cdot\frac{(\bar{V}_1/\bar{V}_0) - (\bar{U}_1/\bar{U}_0)}{1 + (\bar{V}_0/\bar{U}_0)^2}\right]_i + 0(\epsilon^2) \quad (37)$$

III. Particle Heating

With the solution for the particle trajectories in the body stagnation region in hand, we can now proceed to estimate the aerodynamic heating of the particles. Since a significant fraction of the particle mass may be heated to the melting point, it is appropriate to examine any broad assumptions that may be made regarding the rather complicated details of the melting process. To allow a relatively simple solution, we have assumed that the particle material immediately reaches the melting temperature, liquefies, absorbs its latent heat, and is immediately swept away without altering the local heat-transfer rate. In this way our analysis probably overestimates the particle material lost by melting. Note, however, that this simplifying assumption is not unrealistic in view of both the very large shear felt by the melted material and the substantial centrifugal forces due to the large spin rates likely to be caused by asymmetries in the small particles.

To complete our ablation analysis we further assume that the particles are spheres heated only over their front halves at some average rate q, and that they retain their spherical shape as they melt. With these assumptions, net energy conservation for a particle subjected to an average heat rate q over the front face gives

$$2\pi r^2 q = -\sigma Q 4\pi r^2 dr/dt \quad (38)$$

where $Q = C_p (T_{fus} - T_\infty) + Q_{lat}$ is the sum of the heat capacity of the particle material from its initial temperature to fusion temperature and the latent heat of fusion.

For the Reynolds numbers of interest here, the heating of the front face is laminar, and we can estimate[8] that $q = 0.53\ q_{stag}$, where q_{stag} is the stagnation point heating rate. The function q_{stag} can be obtained by correlating the experimental results of Rose and Stark,[9] since their shock tube experiments precisely simulate the doubly shocked environment of the drop traversing a shock layer. Such a correlation yields

$$q_{stag} = E/r^{1/2} \quad (39)$$

where

$$E \cong 2(\rho_\infty/\rho_0)^{1/2} M_\infty^{3.5} [\text{Btu/ft}^{3/2}\ \text{sec}] \quad (40)$$

These equations yield the steady stagnation-point heating for a particle that is not decelerated in the body shock layer. To account for this deceleration effect, we write the speed-dependent, average heating rate to the particle as

$$q = 0.53\ q_{stag}(-\bar{U})^3 \quad (41)$$

For the purpose of the heating calculation along the stagnation streamline, we employ the solution for $\bar{U}_0$ given by Eq. (13).

As before, we replace t by y as the independent variable. Let $\bar{r} = r/r_e$, where r_e is the initial radius of the particle. Then, substituting Eq. (41), Eq. (38) can be written

$$\bar{r}^{1/2} d\bar{r}/dy = -0.265 H_e \exp(-2K_{se}y/\bar{r}) \quad (42)$$

where the dimensionless group H_e is defined as

$$H_e = E\Delta/\sigma Q V_\infty r_e^{3/2} \quad (43)$$

and where K_{se} is defined by Eq. (4) with $r = r_e$.

Equation (42) has been integrated numerically for various values of H_e and K_{se}. The results for $\bar{r}_i$ are shown in Fig. 4, and $\bar{U}_i = -\exp(-K_{se}/\bar{r}_i)$ is shown in Fig. 5. Note that for H_e greater than about 6, the particle has very little velocity at impact. For small values of K_{se}, $\bar{r}_i \approx (1 - 0.398\ H_e)^{2/3}$, which vanishes for $H_e = 2.52$. For values of H_e greater than 2.52, $\bar{U}_i$ goes to zero instead of unity for small K_{se}; but this behavior is not physically significant since the assumption $C_D = \text{const}$ breaks down for extremely small particles.

For particles that are only slightly melted, we can interpret H_e as the total aerodynamic heating received by the particle while traversing the shock layer divided by the total heat capacity (including latent heat) of the particle.

In this analysis we have neglected radiative heating, since although the temperature and density in the particle's shock layer can be very high, the radiating volume is generally small. Estimates were made under typical conditions of the thermal radiation to the particle from its shock layer and from the body shock layer. These estimates indicated the radiative heating from both sources was much less than the convective heating.

In principle this melting calculation can be carried out in the conical region as well. However, as a practical matter, conditions in the conical shock layer are generally not sufficiently severe to cause significant particle melting.

IV. Particle Breakup

We now consider the situation in which the particles overtaken by the shock layer are initially liquid, as when a vehicle

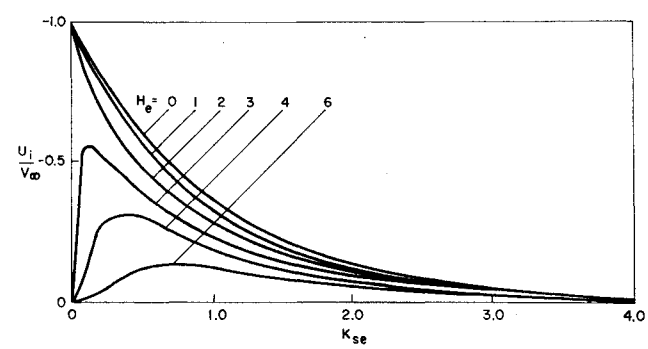

Fig. 5 Particle velocity at impact, including mass loss by heating.

flies through rain. In addition to being decelerated, deflected, and heated as they traverse the shock layer, liquid drops are distorted and shattered by the air flow behind the shock wave. We shall treat this problem in the context of the zero-order solutions discussed in Sec. II to the extent that aerodynamic properties will be assumed constant between body and shock. As will be seen later, this assumption is consistent with the experimental data upon which the drop shattering analysis is based. Since the distortion of the drops increases their drag to several times the initial (spherical) drop drag, however, thereby making C_D a function of time, we shall use experimental results for the drop deceleration rather than calculating it.

Shock tube studies particularly relevant to this problem have been reported by Nicholson[4] and Ranger and Nicholls.[5] Both studies employed a shock tube to measure the time required for drops falling across the tube to be shattered by the flow behind the shock wave. The experiment is sketched in Fig. 6 in room fixed coordinates. The distance s behind the shock wave in which the drop is shattered is given by

$$s = u_s t - x$$

This equation can be rewritten in dimensionless form as

$$\frac{s}{2r} = \frac{tu_2(\rho_2/\sigma)^{1/2}}{2r}\left[\frac{\epsilon^{1/2}}{b^{1/2}(1-\epsilon)}\right] - \frac{x}{2r} = T\frac{\epsilon^{1/2}}{b^{1/2}(1-\epsilon)} - X \tag{44}$$

where T and X are defined by the last equation, where $\epsilon = \rho_\infty/\rho_2$ (as just seen) and $b = \rho_\infty/\sigma$, and where we have used the fact that, in this coordinate system, $u_2/u_s = 1 - \epsilon$. The significant experimental result of the two cited studies was that both the dimensionless groups T and X were constant and independent of the test conditions u_s, ρ_∞, and r. Therefore s/r depends only on the parameters ϵ and b. This experimental result preserves the similitude discussed in Sec. II with the exception that a new parameter b has been added. This new parameter is altitude dependent through ρ_∞. Thus for any given flight conditions, the distance behind the shock wave in which a drop is shattered is proportional to the drop's initial radius.

Before continuing, the limitations on the test data should be enumerated and emphasized. The shock Mach number in the tests was 3.5 or less, the initial density was atmospheric or less, the drop diameters ranged from 0.9 to 2.7 mm, and air and water were the only tested fluids. Therefore, use of the data for smaller drops or higher shock Mach numbers is speculative, as is the effect on the quoted correlation of the liquid density σ. Moreover, although the drop loses mass due to the stripping action of the air more or less continuously after shock passage, only the time at which the drop was totally shattered was determined. Finally, the criterion for what constituted a "shattered" drop was different in the two experiments.

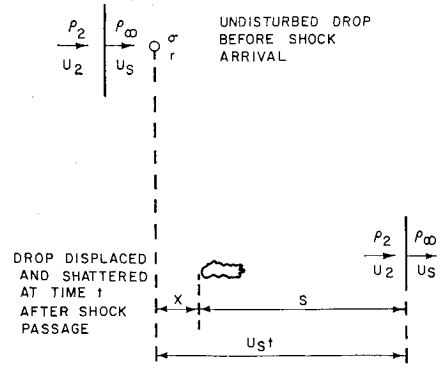

Fig. 6 Shock tube drop shattering experiment.

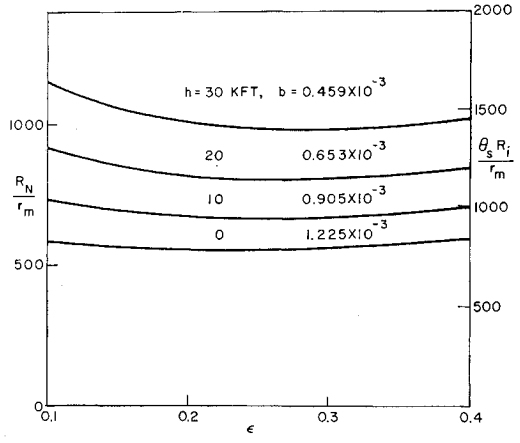

Fig. 7 Drop breakup in stagnation line and conical flow.

Based on their test data, Nicholson[4] reports $T = 3.49$ and $X = 12.1$, whereas Ranger and Nicholls[5] report 5.0 and 27.5, respectively. Clearly, the shattering criterion used by Ranger and Nicholls corresponds to a later stage of drop erosion than that of Nicholson.

Returning to the question of the drop traversing a shock layer about a vehicle and referring to Fig. 1, we note that the drop of initial radius r for which s just equals Δ (in the stagnation region) or L (in the conical shock layer) is the minimum initial size drop that will strike the body at those points. Smaller drops will be entirely shattered before reaching the surface. Noting that

$$L = R_i \sin(\theta_s - \theta_c)$$

and defining

$$B = \epsilon^{1/2}/b^{1/2}(1-\epsilon) \tag{45}$$

we have for the stagnation region

$$\Delta/r_m = 2(BT - X) \tag{46}$$

and for the conical region

$$R_i/r_m = 2(BT - X)/\sin(\theta_s - \theta_c) \tag{47}$$

where r_m is the initial radius of the smallest drop that will hit the stagnation point or the longitudinal location R_i on the cone, respectively.

Note that in the shock tube experiments, the gas state behind the shock wave is constant. Thus, equating s with Δ neglects the variation in gas speed and density between shock wave and body stagnation point. Similarly, equating s with L is strictly correct only for flow over a wedge, in which flow properties are invariant between the shock and the body. (In drop-fixed coordinates this wedge flow corresponds to the flow behind a normal shock of speed $M_\infty \sin\theta_s$, with a corresponding value of ϵ for the oblique shock.) It is in this sense that the drop shattering analysis corresponds to the zero-order solutions presented in Sec. II. In view of the nature of the shock tube experiments, no simple improvement can be made to account for gas property variations in the actual shock layer surrounding a body.

We can further simplify the above equations by making use of the high-speed correlations (8) and (25) for standoff distances given in Sec. II, with $\xi_\Delta = 0.78$ and $\lambda_\theta = 0.6$. The stagnation point solution then becomes

$$R_N/r_m = (2.56/\epsilon)(BT - X) \tag{48}$$

and, making the small angle approximation, the cone solution is

$$\theta_s R_i/r_m = (3.64/\epsilon)(BT - X) \tag{49}$$

These two functions are plotted vs ϵ for various values of b in Fig. 7 using the empirical values of T and X reported by

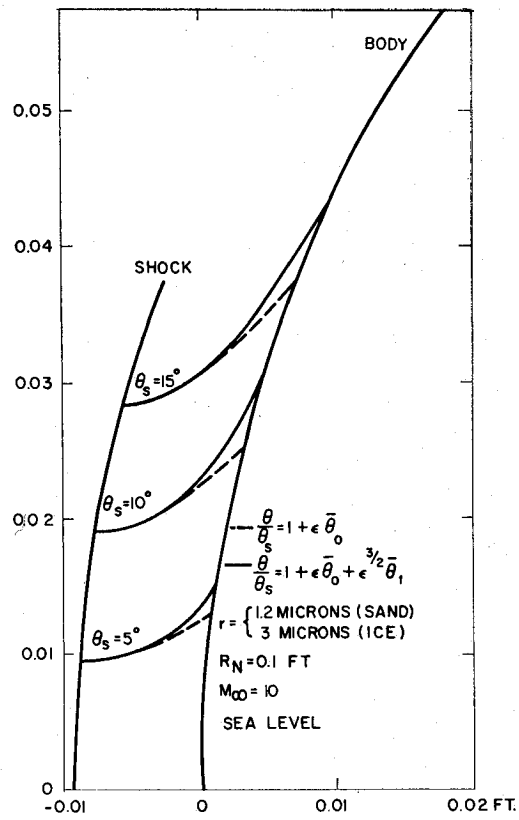

Fig. 8 Particle trajectories, R_N = 0.1 ft.

Nicholson. Assuming that the liquid drops are water, ρ_∞ and, hence, the altitude h, are specified by each value of b as noted in Fig. 7.

Recent experimental work[10,11] has been carried out at higher shock Mach numbers, yielding a better simulation of conditions in the shock layers of high-speed vehicles. This work substantiates the empirical value of T reported by Nicholson for the lower shock Mach numbers but suggests that a different mechanism of drop breakup may become important for higher shock Mach numbers,[11] in which the value of T at breakup is a function of the local Weber number. For this reason, the results shown in Fig. 7 for values of ϵ less than about 0.2 may not be valid for certain combinations of vehicle configuration and drop size. The effect of the more recent data presented in Refs. 10 and 11 on drop breakup in high-speed shock layers will be explored in a subsequent report.

V. Numerical Calculations

In order to illustrate the relative importance of shock-layer effects, we have considered the particular case of a 10° half-angle cone blunted by a 0.1-ft nose radius. The flight conditions are $M_\infty = 10$ at sea level.

Ballistic coefficients for the nose and cone regions were calculated from the formulas

$$K_s = (3C_D\rho_\infty/8\sigma)\xi_\Delta R_N/r, \quad K_c = (3C_D\rho_\infty/8\sigma)\lambda_\theta\Theta_s R_i/r$$

For the stagnation region, the capture area ratio and impact angle for unmelted ice and sand particles of various radii have been indicated on Figs. 2 and 3, with $\epsilon = 0.12$ in this case. The drag coefficient C_D was assumed to be unity; for the sand particles, we took $\sigma = 4.85$ slugs/ft^3. Although the effects shown are relatively small for this nose radius, it should be noted that a 10-μ-radius ice particle, for example, would impact with about one-third the freestream velocity according to Eq. (13), independent of melting effects, a significant loss of energy.

Typical particle trajectories in the nose region are illustrated in Fig. 8. For the nominal 0.1-ft nose radius, these are the trajectories of either 3-μ-radius ice particles or 1.2-μ-radius sand particles. For a larger 0.5-ft nose radius, the scaled particle radii would be 15 and 6 μ, respectively. Equations (17) and (18) have been employed in these computations.

For the conical-flow region, Fig. 9 shows the capture area ratio and impact angle as functions of K_c and illustrates the values of these quantities for ice and sand particles striking the body at a point 10 ft downstream from the nose. We note that for $\theta_c < 20°$, terms containing $\theta_c \tan\theta_c$ and $\tan^2\theta_c$ are negligibly small in β and $\bar{R}_2$, so that with $\lambda_u = 0$ we have

$$\beta \cong \tan^{-1}(e^{-K_c}\tan\theta_c) + \epsilon e^{-K_c}\tan\theta_c \times \{2[(e^{K_c}-1)/K_c - 1] - \lambda_\rho K_c/2 - \lambda_\theta\theta_c\cot\theta_c \times [(2-K_c)(e^{K_c}-1)/K_c - 2]\}$$

$$\bar{R}_2(0) \cong (\lambda_\theta\theta_c\cot\theta_c/K_c^2)\{(1-\lambda_\theta\theta_c\cot\theta_c)\{K_c + \tfrac{1}{2} + [\tfrac{3}{2}e^{K_c} - 2(K_c+1)]e^{K_c}\} + K_c\lambda_\theta(e^{K_c}\theta_c\cot\theta_c - 1)(e^{K_c}-1) + (\lambda_\rho/2)[2 - (K_c^2 - 2K_c + 2)e^{K_c}]\}$$

In Fig. 9 we have taken $\epsilon = 0.35$. Since the convergence of the series for $\bar{R}(0)$ in ϵ was poor for $K_c > 1$ in this case, we

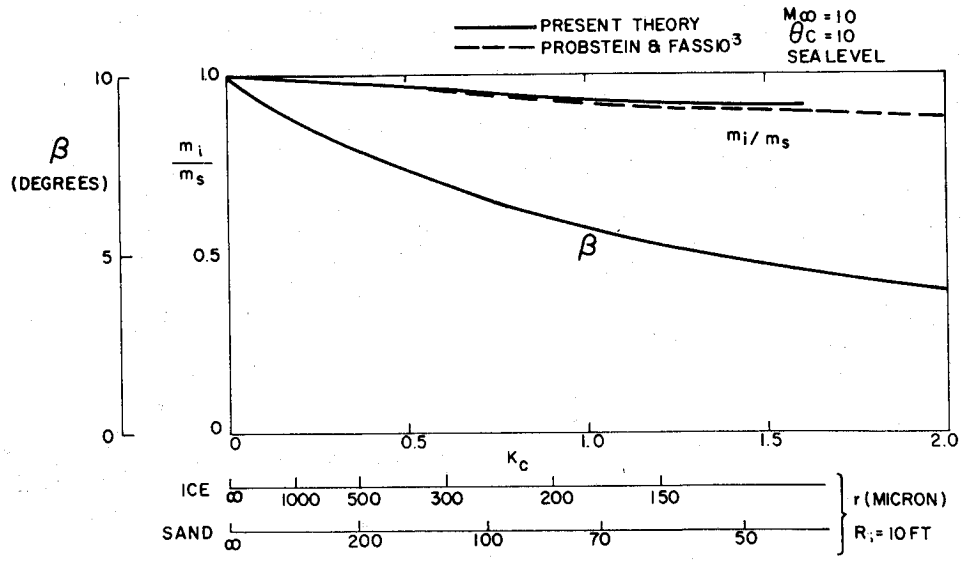

Fig. 9 Capture area ratio, impact angle for 10° cone.

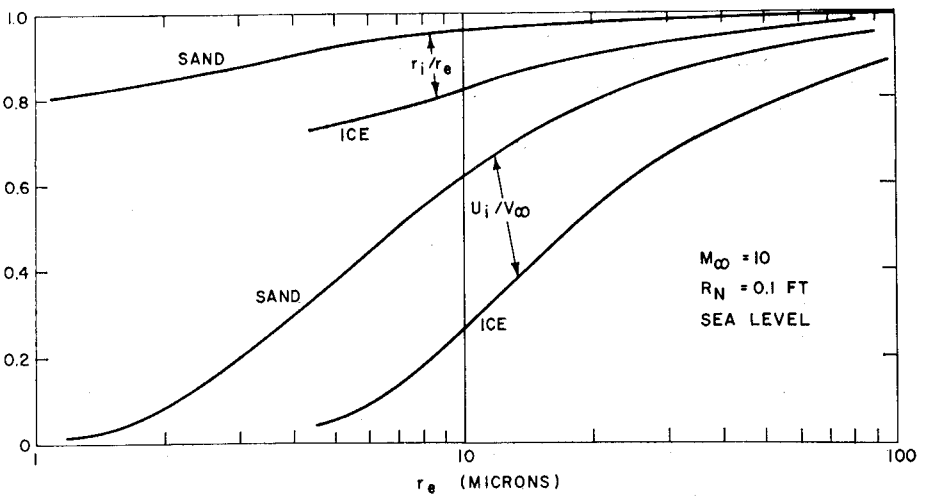

Fig. 10 Stagnation line: particle radius and velocity at impact including melting, R_N = 0.1 ft.

expressed the series as a rational fraction following Shanks[12]:

$$\frac{m_i}{m_s} \simeq \left(\frac{1}{1-\epsilon\lambda_\theta}\right)^2 \left\{\frac{\bar{R}_1(0) + \epsilon[\bar{R}_1^2(0) - \bar{R}_2(0)]}{\bar{R}_1(0) - \epsilon\bar{R}_2(0)}\right\}^2$$

The results for the capture area ratio shown in Fig. 9 agree well with those of Probstein and Fassio,[3] and indicate that in general the impact angle is a more sensitive parameter for assessing particle deflection effects in the conical shock layer. Figure 9 shows that deflection effects in the conical shock layer can be important even for relatively large particles.

The effects of particle melting in the stagnation region of the 0.1-ft-radius nose are shown in Fig. 10. In these calculations we took Q = 8000 Btu/slug for ice and Q = 24,000 Btu/slug for sand. The computations are based on the solution shown in Figs. 4 and 5, which takes into account the combined effects of deceleration and particle mass loss due to melting. Although the reductions in particle radius due to heating that are shown in Fig. 10 are generally quite small, the mass reductions are proportional to the cube of the radius and hence are more substantial. We observe that sand particles of 2 μ radius and ice particles of 6 μ radius lose all but 8% of their impact velocity, whereas sand particles of 7 μ radius and ice particles of 18 μ radius lose half their impact velocity.

To illustrate the significance of the drop shattering phenomenon, we observe that in the stagnation region we get r_m = 50 μ from Eq. (48) using the empirical values for T and X given by Ranger and Nicholls[5]; we get r_m = 53 μ using Nicholson's values.[4] Hence it appears in either case that water drops less then 0.1 mm in diameter will be shattered before reaching the body surface in the nose region. It follows that rain drops will be generally unaffected, whereas cloud droplets, whose radius is about 10 μ, will not reach the body surface. This conclusion should be qualified, however, by noting that this calculation extends the data correlation well beyond its empirical range.

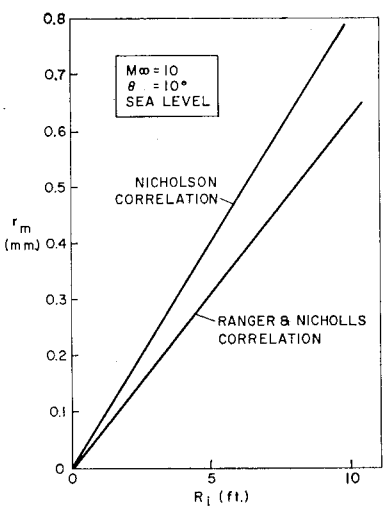

Fig. 11 Water drop shattering for 10° cone.

In the conical region, the initial size of the smallest drop that will hit the body depends on the slant distance to the point of impact R_i. This is illustrated for the 10° cone in Fig. 11, based on Eq. (49). Note that since most raindrops are of the order of 1 mm in diameter, few raindrops will reach the cone surface aft of the 7-ft station.

VI. Conclusions

Approximate, closed-form results have been presented for the deceleration, deflection, melting (or vaporization), and shattering of small spherical particles, either solid or liquid, in the flow field around a high-speed body. The analytical approach has been to express the pertinent quantities in series in the small density ratio across the bow shock wave. In the stagnation region, the trajectory of a particle depends on the parameters ϵ and K; the mass loss due to heating introduces the additional parameter H_e, and the shattering depends as well on the parameter b. In the conical flow region, the half-angle of the cone θ_c becomes a parameter.

Based on the analysis, calculations have been carried out for a particular configuration traveling at Mach 10 at sea level. The effects of particle deflection in the stagnation region for a 0.1-ft radius nose are small except for very tiny particles, but the deceleration effects are substantial for ice particles with radii on the order of 10 μ. Relatively little material is removed by melting of ice and sand particles larger than about 10 μ in radius for this case, so that the effects of melting are minimal. On the other hand, raindrops smaller than about 50 μ radius will be completely shattered in the nose region.

In the conical-flow region, deflection effects are very important. For a 10° half-angle cone, the impact angle 10 ft downstream of the nose is reduced to 5° for ice particles smaller than about 150 μ radius and sand particles smaller than about 60 μ radius. There is no solid-particle melting in the conical shock layer. Raindrops smaller than about 700 μ radius, which would strike the cone 10 ft downstream of the nose in the absence of a shock layer, will be completely shattered by the relative flow in the shock layer, so that very little rain will reach the cone surface downstream of this station.

References

[1] Taylor, G. I., "Notes on Possible Equipment and Techniques for Experiments on Icing on Aircraft," R and M 2040, 1940, Aeronautical Research Committee, London.

[2] Reinecke, W. G. and Waldman, G. D., "Particle Trajectories, Heating, and Breakup in Hypersonic Shock Layers," AIAA Paper 69-712, San Francisco, 1969.

[3] Probstein, R. F. and Fassio, F., "Dusty Hypersonic Flows," *AIAA Journal*, Vol. 8, No. 4, April 1970, pp. 772–779.

[4] Nicholson, J., "Drop Breakup by Airstream Impact," *Rain Erosion and Associated Phenomena*, Rept. N68-19401-427, 1967, Royal Aircraft Establishment, Farnborough, England, pp. 342–369.

[5] Ranger, A. and Nicholls, J., "Aerodynamic Shattering of Liquid Drops," *AIAA Journal*, Vol. 7, No. 2, Feb. 1969, pp. 285–290.

[6] Inouye, M., "Shock Standoff Distance For Equilibrium Flow Around Hemispheres Obtained From Numerical Calculations," *AIAA Journal*, Vol. 3, No. 1, Jan. 1965, p. 172.

[7] Seiff, A., "Recent Information on Hypersonic Flow Fields," *Gasdynamics in Space Exploration*, SP-24, NASA, 1962.

[8] Lees, L., "Laminar Heat Transfer over Blunt-Nosed Bodies at Hypersonic Flight Speeds," *Jet Propulsion*, Vol. 26, April 1956, p. 259.

[9] Rose, P. H. and Stark, W. J., "Stagnation Point Heat Transfer Measurements in Dissociated Air," *Journal of the Aerospace Sciences*, Vol. 25, Feb. 1958, p. 86.

[10] Reinecke, W. G. and McKay, W. L., "Experiments on Water Drop Breakup Behind Mach 3 to 12 Shocks," AVATD-0172-69-RR, June 1969, Avco Corp., Wilmington, Mass.

[11] Reinecke, W. G. and Waldman, G. D., "An Investigation of Water Drop Disintegration in the Region Behind Strong Shock Waves," 3rd International Conference on Rain Erosion and Related Phenomena, Hampshire, England, Aug. 1970.

[12] Shanks, D., "Non-linear Transformations of Divergent and Slowly Convergent Sequences," *Journal of Mathematics and Physics*, Vol. 34, 1955, pp. 1–42.

JUNE 1971 AIAA JOURNAL VOL. 9, NO. 6

A Unified Analysis of Gaseous Jet Penetration

F. S. Billig,* R. C. Orth,† and M. Lasky‡
The Johns Hopkins University, Applied Physics Lab., Silver Spring, Md.

The strengths and weaknesses of various physical and mathematical concepts that have been employed in the development of theories concerning transverse gaseous jet penetration into a supersonic stream are discussed in relation to the latest experimental results reported in the literature. A new unified model that provides excellent agreement with measured flow field properties is presented. The development of this model rests on the similarity that exists between a jet discharging into a quiescent medium and a jet discharging into crossflow. By the suitable definition of an "effective back pressure," a correlation is obtained between the normal distance to the center of the Mach disk and the ratio of injection pressure to effective back pressure. Other correlations are used to obtain the size and shape of the initial portion of the jet, which permit the calculation of a) the complete trajectory of the injectant and b) a one-dimensional approximation of the mass-averaged properties at any point along the trajectory downstream of the Mach disk.

Nomenclature

A = area
A_p = projected area
C_p = pressure coefficient = $(p - p_a)/q_a$
C_p^* = stagnation pressure coefficient defined by Eq. (6b)
D = jet diameter
D_j^* = diameter of jet orifice at sonic point
F_N = normal force on jet element (Fig. 8)
F_x = defined as $\int_{A_x} p dA$
h = enthalpy [Eq. (4)]
h = radius of quarter sphere-half cylinder injection model
h' = diameter of spherical nosed cylinder injection model
$\tilde{h}$ = ordinate of jet center of mass
K = constant defined in Eq. (42)
m = mass
M = Mach number
p = pressure
p_{eb} = effective back pressure = $\frac{2}{3}p_{t'a}$
p_t' = pitot pressure
p_j^* = pressure at sonic point in jet orifice
q = dynamic pressure = $\rho u^2/2$
r = jet radius
R_c = local radius of curvature for jet trajectory
s = distance along jet trajectory
T = temperature
u = velocity
W = Mach disk diameter (Fig. 8)
x = axial distance measured from center of injection port
y = normal distance from point of injection
y_1 = normal distance to center of Mach disk (Fig. 4)
$\bar{y}$ = maximum ordinate of Mach disk (Fig. 8)
z = lateral distance measured from center of injection port
α = local angle of freestream flow (Fig. 1)
$\hat{\alpha}$ = defined in Eq. (27) (Fig. 8)
δ = local angle of jet centerline (Fig. 1)
$\hat{\delta}$ = local angle of jet surface in plane of symmetry
Γ = function defined by Eq. (12b)
γ = ratio of specific heats

Superscript

$(\bar{\ })$ = averaged one-dimensional property at a particular station

Subscripts

a = undisturbed freestream conditions at upstream edge of control volume (Fig. 1)
b = freestream conditions at downstream edge of control volume (Fig. 1)
c = jet stream conditions at downstream edge of control volume (Fig. 1)
j = jet conditions at point of injection (Fig. 1)
j_1 = jet diameter for $p_{tj}/p_{ta} = 1$ (Fig. 11)
A_x = axial direction of surface integration on jet-freestream boundary (Fig. 1)

Presented as Paper 70-93 at the AIAA 8th Aerospace Sciences Meeting, New York, January 19–21, 1970; submitted August 11, 1970; revision received December 14, 1970. This work was supported by NASA Office of Aeronautical Research, Advanced Research and Technology under Contract N00017-62-C-0604 with the Department of the Navy.

* Supervisor Hypersonic Ramjets Project. Associate Fellow AIAA.
† Engineer, Hypersonic Ramjets Project.
‡ Associate Mathematician, Hypersonic Ramjets Project.